

COMPARATIVE ANALYSES OF MICRO-PARTICLE IMPACT BETWEEN TRANSONIC AND SUBSONIC AXIAL COMPRESSORS

N. Aldi^{1,a} - *M. Morini*^{2,b} - *M. Pinelli*^{1,c} - *P. R. Spina*^{1,d} - *A. Suman*^{1,e}

¹ Engineering Department in Ferrara (EnDiF), University of Ferrara, Ferrara, Italy

² Department of Industrial Engineering, University of Parma, Parma, Italy

^a nicola.aldi@unife.it, ^b mirko.morini@unipr.it, ^c michele.pinelli@unife.it,

^d pier.ruggero.spina@unife.it, ^e alessio.suman@unife.it

ABSTRACT

Solid micro-particle ingestion is one of the principal degradation mechanisms in compressor sections. In particular, in industrial applications, micro-particles not captured by the air filtration system cause fouling and, consequently, a performance drop.

This paper presents three-dimensional numerical simulations of micro-particle ingestion (0.15 – 2.00) μm on axial transonic and subsonic compressor rotors. The mass flow rate swallowed by the two rotors is comparable and represents the basis for the fouling comparison. The results show that particles tend to follow the flow by impacting on blade tips with a higher concentration on the pressure side. The suction side is affected only by smaller particle impact (up to 1 μm). Fluid-dynamic phenomena such as separation, stagnation point and tip leakage vortex strongly influence the impact location. Guidelines for proper management in terms of air filtration systems and washing strategies of the power plant in which the compressor could be installed are proposed.

NOMENCLATURE

B	bounce (average)	ν	kinematic viscosity
b, C, f	model constant (referred to the Ahlert's model)	ρ	density
d	diameter		
e_n, e_t	normal, tangential restitution coefficients	Subscript	
m	mass flow rate	b	bounce
N	total number	f	filtration system
n	ratio	hit	hit
St	Stokes number	p	particle
u	relative velocity particle	side	side
u_t	shear velocity	TT	total-to-total
y^+	non-dimensional distance		

Greek symbols

α	impact angle
β	total pressure ratio
η	efficiency
τ_w	wall shear stress
τ^+	non-dimensional particle relaxation time

Acronyms

DPM	Discrete Phase Model
DRW	Discrete Random Walk
LE	Leading Edge
PS	Pressure Side
SS	Suction Side
STW	STandard Wall function

INTRODUCTION

Gas turbines ingest a large amount of air during their operation. The quality and purity of the air entering the turbine is a significant factor in the performance and life of the gas turbine. In particular, the fouling of the axial compressor is a serious operating problem and its control is of critical importance for operators of gas turbine-driven power plants, compressor stations and pump stations. In order to minimize the performance loss of industrial gas turbines, an adequate filtration

system that can limit the ingestion of contaminants by the power unit is required. For industrial gas turbines, highly effective filtration systems exist (Wilcox et al., 2011). Because modern inlet filtration systems are effective in removing particles larger than 2 μm , compressor erosion is not a problem frequently found in industrial gas turbines. However, depending on the type of filtration system used, smaller particles can enter the engine. These smaller particles are too small to cause erosion issues, but they do cause compressor fouling.

Evaluation of fouled compressors have revealed contamination both on the suction side and the pressure side of the compressor blades (Kurz and Brun, 2012). Kurz and Brun (2012) also pointed out that only small particles can stick to the blade surface and thus cause fouling. Tarabrin et al. (1998a) reported an investigation of compressor blade contamination for a Nuovo Pignone MS5322 R(B) gas turbine engine. This power unit operated for a long time without blade washing but only the first 5 to 6 stages of 16 are subjected to blade fouling due to deposits. The inlet guide vane blades, as well as the rotor and stator blades of the first stage have more deposits on the blade convex side. The deposits masses on blades of the other stage are approximately equal for the convex and concave side. The deposits masses decrease from the first to the sixth stage. From the seventh stage, the amount of deposits on blades is insignificant. The authors highlighted that the deposits amount is greater on the stator blades, than on the rotor blades due to the cleaning effects provided by the centrifugal forces on a dirt particles. Centrifugal forces have characterized also the results obtained by Syverud et al. (2005). The authors reported the location of salt deposits in General Electric J85-13 axial compressor. The experimental tests have shown that the salt deposits were mainly found along the leading edge of the first four stages and on the pressure side of the stator vanes along the hub. The salt deposits were generated by the salt carried by the water droplets, and for this reason, significantly less deposit were observed on the rotor blades compared to the stator vanes.

The question that still requires research is the mechanism that allows particles to actually reach the suction surface. Particles that deviate from the streamlines will readily impact on the pressure side of the blades, but the mechanism that can deposit particles on the suction side of the blade is not fully understood. The particle sticking on blade surfaces results in an increase of the thickness of the airfoil and the surface roughness. Both of these events change the flow-path inside the passage vanes, in particular: (i) increment of the boundary layer thickness, (ii) decrement of the flow passage area and (iii) modifications of the 3D fluid dynamic phenomena.

In this paper two main issues are referred to: (i) CFD numerical simulations of the particle tracking and (ii) fouling in the axial compressors. In literature there are studies related to the gas turbine and studies related to the axial compressor. Due to the aim of this paper, only the studies related to the compressor are considered. Suzuki et al. (2008) performed a study of the erosion effects in an axial compressor stage. Due to the particle tracking method, the authors took into account the effect of the rebounded particles and the results show that the first impact of the particle determines the most important erosion on the blade surface, in particular at the leading edge. Ghenaïet (2012) studied the particle dynamics and erosion of the front compression stage of a turbofan PW-JT8-D17. Particle trajectory simulations used a stochastic Lagrangian tracking code and the sand particle size varied from 0 μm to 1,000 μm . The numerical simulations show different trajectories for different particle diameters. Larger particles were affected by inertia and centrifugal force and some crossed the blade through the tip clearance and induced erosion of the blade tip. Small size particles (i.e. $\approx 10 \mu\text{m}$) tended to follow the flow path closely and were strongly influenced by the flow turbulence, secondary flows, and flow leakage above the blade tip and induced erosion of the blade tip and shroud.

Experimental results for the fouling issue can be found in Viguera Zuniga (2007) and Parker and Lee (1972). The authors have reported some experimental measurements with regard to the deposition on the axial compressor blade surface. In particular, Viguera Zuniga (2007) reports the deposits on the gas turbine compressor rotor and stator vanes for off/in-shore applications. Parker and Lee (1972) report a study of fouling patterns on blades caused by an ingestion of sub-micron

particles (0.13 – 0.19) μm . While for the experimental evaluation of fouling the data presented in literature cover some applications, from a CFD point of view, there is a lack of study. The fouling phenomena on the axial compressor can be well reproduced by a combined strategy that involves the modification of the thickness of the airfoil and the application of a surface roughness on the blade surface (Morini et al., 2010). With this method, the authors presented some sensitivity analyses related to the different positions of the deposits (pressure and suction side, spanwise direction) on the blade surface by using different values of surface roughness (Morini et al., 2011, Aldi et al., 2014).

In this article, the authors present a CFD study for the ultra-fine powder ingestion (particle size 0.15 – 2.00) μm by a transonic rotor and a subsonic rotor. This work is the consequence of the analysis reported by Suman et al. (2014), in which the CFD numerical analysis was used to define which blade areas are more affected by particle impacts.

The results show the position and the quantity of the ingested particles that affected the blade surface of two different axial compressor rotors. Even if, in the last decade, manufacturers have been oriented to the development of transonic axial compressors, subsonic stages are commonly used for heavy-duty industrial applications such as pump stations and process compressors thanks to their very high reliability and relatively restrained cost (maintenance and recovery).

Theoretically, zones with a high number of impacts will be more affected by the fouling phenomena, but, actually, the fouling phenomena depend only on the sticking characteristic of the particles. However, the differences in the particle impact pattern lead directly to the fouling phenomena. The particle ingestion was studied by using a CFD commercial code. The main items of this work can be summarized as follows: (i) validation of the numerical models by using the experimental and numerical data reported in literature, (ii) simulation of the ingestion of a fine powder characterized by different particle diameters, and finally, (iii) quantitative and sensitivity analysis of the particle impact and evaluation of the contaminant concentration on the blade surfaces. Particular attention was given to the particle impact pattern on the blade surface. In this paper particular emphasis was placed on (i) the sensitivity analysis related to the boundary layers, since the turbulent eddy structures are suspected to contribute to the impact of particles on the blade surface and (ii) the differences between the particle impact pattern of the two considered rotors.

NUMERICAL DOMAIN AND COMPRESSOR PERFORMANCES

The numerical simulations were carried out by means of the commercial CFD code ANSYS Fluent 13.0. The code solves the 3D Reynolds-averaged form of the Navier–Stokes equations by using a finite-element based finite-volume method. An implicit Roe-Flux-Difference Splitting (FDS) formulation was adopted with a Green-Gauss Node Based spatial discretization. For the flow, a second order Upwind was chosen. The standard $k-\varepsilon$ turbulence model with a STandard Wall function (STW) was used. For the turbulent terms, a first order Upwind scheme was adopted for the solution phase. All the simulations were performed in a steady multiple frame of reference by using a frozen rotor interface. In fact, the mixing plane approach as implemented in ANSYS Fluent does not allow particle tracking through different domains. However, the numerical domains used in this work are not affected by the rotor stator interaction and, for this reason, the frozen rotor strategy is considered suitable for this study. Each numerical domain is composed of three domains: two stationary domains (inlet and outlet duct) and one rotating domain (rotor).

Transonic rotor

The transonic rotor is the NASA Rotor 37 (Reid and Moore, 1978). It is composed of 36 blades but only a single passage vane was modeled. The hub to tip ratio is equal to 0.705, while the tip clearance at design speed is 0.356 mm (0.45 % of the blade span). The transonic rotor is studied at its nominal rotational speed equal to 17,188 rpm and the peripheral velocity at the blade tip is equal to 454 m/s that corresponds to a rotor tip Mach number equal to 1.34. A multiblock hexahedral grid with a total number of 1,131,063 elements was used. Regarding the near walls, the nodes are

positioned in such a way that the values of y^+ are within 5 – 65.

Subsonic rotor.

The subsonic rotor is the first stage of a multi-stage axial compressor used in industrial applications. It is composed of 31 blades but only a single passage vane was modeled. The hub to tip ratio is equal to 0.739, while the tip clearance is 0.382 mm (0.45 % of the blade span). The subsonic rotor is studied at its nominal rotational speed equal to 6,054 rpm and the peripheral velocity at the blade tip is equal to 206 m/s that corresponds to a rotor tip Mach number equal to 0.62. A multiblock hexahedral grid with a total number of 1,007,800 elements was used. Regarding the near walls, the nodes are positioned in such a way that the values of y^+ are within 5 – 71.

Boundary conditions.

For both rotors, the inlet total pressure and total temperature were imposed at 101,325 Pa and 288.15 K, respectively. An average static pressure p_2 was imposed at the outflow boundary, both in the near-choked flow region and in the near-stall region. The outflow pressure p_2 was progressively increased (from the near-choked flow region to near-stall region) in order to perform the entire performance trends. The inlet surface mesh has every single element with the same size in order to guarantee a uniform node distribution on the surface. The uniform distribution of grid nodes allows the realization of a uniform particle injection from this surface. The inlet surface is composed of 1,888 and 2,596 elements for the transonic and subsonic rotor respectively. The performance trends in terms of total pressure ratio β , the total-to-total efficiency η_{TT} and the blade shape are reported in Figure 1. In the case of transonic rotor, the numerical results correctly reproduced the experimental one provided by Reid and Moore (1978) (not reported here). The numerical total pressure ratio β and the total-to-total efficiency η_{TT} always underestimate the experimental data but in a very consistent way. The deviation in terms of mass flow rate at the choked-flow condition is about 1.87 %. Regarding the subsonic rotor, no experimental data is available. Since the aim of the validation was to obtain a compressor model, the numerical model can be considered reliable. Considering that the subsonic numerical model and its set-up is realized in agreement with those provided for the transonic rotor, it can be state that also the CFD numerical solution obtained for the subsonic rotor is suitable for the aim of the study.

NUMERICAL MODEL: PARTICLE TRACKING AND WALL CONDITIONS

In this paper, the solution approach is based on a mathematical model with Eulerian conservation equations in the continuous phase and a Lagrangian frame model to simulate a discrete second phase (DPM). The airflow field is first simulated, and then the trajectories of individual particles are tracked by integrating a force balance equation on the particle. The force balance is consisting of inertia, drag and buoyancy term. In the force balance there are two contributions due to the shear stress and diffusion called Saffman’s lift force and Brownian force respectively. These last

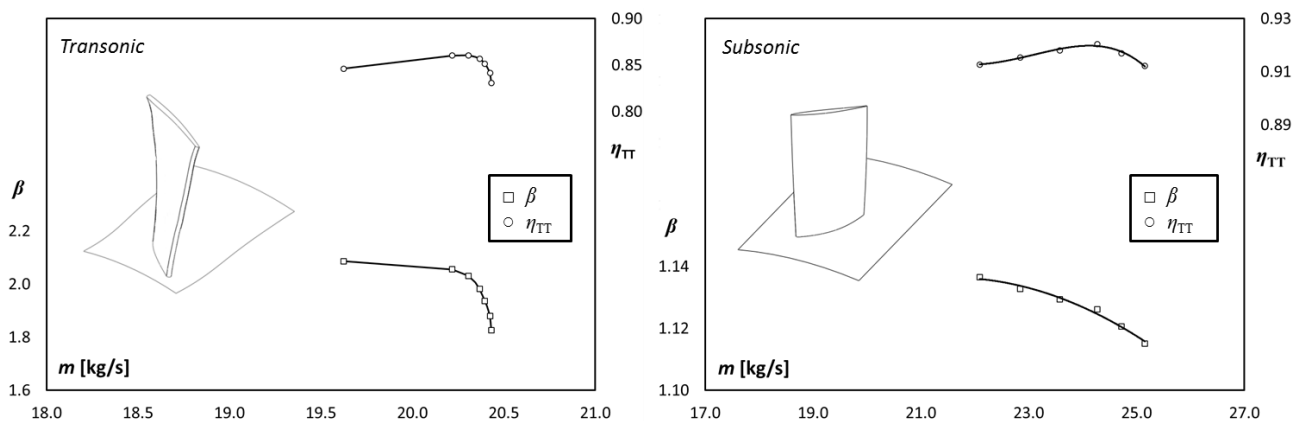


Figure 1 – The performance trends

contributions are generally at least two magnitudes smaller than the drag force. However, some of these forces may occasionally become comparable in magnitude to the drag force within the turbulent boundary layer, but the Brownian term is intended only for laminar simulations and its contribution has not been taken into account in this analysis. The dispersion of particles in the fluid phase can be predicted by using a stochastic tracking model. The time-averaged flow field determines the mean path of particles, while the instantaneous flow field governs each particle's turbulent dispersion from the mean trajectory. By computing the trajectory in this manner for a sufficient number of representative particles (named *number of tries*), the random effects of turbulence on the particle dispersion can be included. This investigation used the Discrete Random Walk (DRW) model to simulate the stochastic velocity fluctuations in the airflow (Gosman and Ioannides, 1983). The number of trajectories was selected in order to satisfy the statistical independence since the turbulent dispersion is modeled based on a stochastic process. In this paper, 1,500 tries for the transonic rotor and 1,100 tries for the subsonic rotor were chosen after a sensitivity analysis. Every single analysis (related to a fixed particle diameter) was carried out with 3 different runs. These values (number of tries and runs) determine almost 8.5 million starting particles at the rotor inlet for each particle diameter.

The DRW model may give non-physical results in strongly non-homogeneous diffusion-dominated flows, where small particles should become uniformly distributed. Instead, the DRW will show a tendency for such particles to concentrate in low-turbulence regions of the flow due to the boundary layer treatment provided by the turbulence model. For these reasons a specific analysis was conducted related to the interaction between the turbulence model and the particle characteristics.

Through the use of $k-\varepsilon$ turbulence model with STW, there is an isotropic treatment of the turbulence near the wall and this implies, in the case where the values of y^+ are less than 5, that both the streamwise mean velocity and the turbulence kinetic energy will be overestimated. More details can be found in Tian and Hamadi (2006). In this paper, the values of y^+ do not drop below 5.

According to the aforementioned detailed work, to investigate in greater detail the relationship between turbulence models, mesh refinement close to the wall and particle dimensions, it is possible to calculate the non-dimensional particle relaxation time τ^+ defined as

$$\tau^+ = \left[(\rho_p / \rho) d_p^2 u_t^2 \right] / 18\nu^2 \quad (1)$$

where the u_t is the shear velocity, $u_t = (\tau_w / \rho)^{1/2}$ and τ_w is the wall shear stress. Tian and Hamadi (2006) highlighted the effect of a different turbulence model on the velocity deposition for particles in a horizontal and vertical tube. Their study has shown that the $k-\varepsilon$ turbulence model with STW over-predicts the deposition velocity for particles in a Brownian ($\tau^+ < 10^{-2}$) and transition ($10^{-2} < \tau^+ < 10$) region and it does not allow the estimation of the real trend of the particle velocity deposition. For the inertial ($\tau^+ > 10$) region, the $k-\varepsilon$ STW turbulence model over-predicts the deposition velocity but in a minor way compared to the other regions and the trend of the deposition velocity curve is in agreement with the other results. As can be seen in Table 1, the non-dimensional particle relaxation time τ^+ , defined by Eq. (1), is in the range 1 – 410 which corresponds to the transition and inertial region. However, the values in the transition region are close to the inertial region and thanks to the analyses mentioned above (values of y^+ and τ^+) the $k-\varepsilon$ STW turbulence model used for all the analyses was considered suitable for studying the real deposition phenomenon that occurs in the axial compressors under investigation.

For the particle-wall interaction boundary conditions, the following conditions have been adopted: (i) ideal adherence condition on the blade surfaces and (ii) non-adherence condition on the hub and shroud surfaces. These conditions allow the evaluation of where and how the contaminants encounter the blade surface for the first time, avoiding the introduction of inaccuracies due to the use of bounce models not fully representative of the real conditions. To set up the DPM the authors have implemented specific functions and restitution coefficients. In particular, the model functions are defined in agreement with Ahlert (1994), where the impact angle function $f(\alpha)$ is defined as

Table 1 – Injection characteristics (d_p [μm], η_f [%], m_p [kg/s])

	Transonic rotor						Subsonic rotor					
d_p	0.15	0.25	0.50	1.00	1.50	2.00	0.15	0.25	0.50	1.00	1.50	2.00
St	4e-4	1e-3	4e-3	2e-2	4e-2	6e-2	3e-4	8e-4	3e-3	1e-2	3e-2	5e-2
τ^+	2	6	26	103	231	410	1	3	13	52	117	209
η_f	61	60	65	85	96	99	61	60	65	85	96	99
m_p	7.4e-7	3.5e-6	2.5e-5	8.4e-5	7.6e-5	4.5e-5	9.8e-7	4.7e-6	3.3e-5	1.1e-4	1.0e-4	6.0e-5

$$f(\alpha) = 17.9\alpha - 33.4\alpha^2 ; 0 < \alpha \leq \pi/12 \quad (2)$$

$$f(\alpha) = 2.1843 + 1.0362\alpha + 0.5777\alpha^2 - 2.8201\alpha^3 + 1.4242\alpha^4 + 0.0618\alpha^5 - 0.1041\alpha^6 ; \pi/12 < \alpha \leq \pi/2 \quad (3)$$

The impact angle α is expressed in radians. The other model constants are related to the material properties (carbon steel and sand): (i) the coefficient for the relative particle velocity $b(u)$ equal to 1.73 and (ii) the coefficient of the particle diameter $C(d_p)$ equal to 1.85e-08. These coefficients are based on direct impingement tests at various angles and impingement velocities provided by Ahlert (1994). The coefficients were calculated through the erosion rate calculation. Ahlert (Ahlert, 1994) proposed the relationship between the erosion rate and some characteristics related to the materials, particle's dimensions and shapes.

The theory of collision indicates that the coefficient of restitution, or the ratio of relative velocities (particle velocity after collision divided by particle velocity before collision), may have any value from one, for completely elastic collision, to zero, depending on the material, size, shape and relative velocity of the colliding bodies. Coefficient of restitution depends not only to the material of the particle but also depends on the direction of the collision. Oblique collision generates friction force and, if the particle has a rotational velocity, the combination of particle rotation with the oblique direction changes the particle trajectories after the collision. Fuchs (1964) have reported some of experimental results provided by different tests. For the restitution coefficients, the results obtained by Forder et al. (1998) were chosen. In this study, the authors found the restitution coefficients for sand particles impacting steel plates. The restitution coefficients are dependent on the particle impingement angle α , and both the perpendicular and tangential components of the restitution coefficients should be considered. Forder et al. (1998) provided the following correlations for both perpendicular e_n , and tangential e_t , restitution coefficients based on impingement testing using AISI 4130 carbon steel and sand

$$e_n(\alpha) = 0.988 - 0.780\alpha + 0.190\alpha^2 - 0.024\alpha^3 + 0.027\alpha^4 \quad (4)$$

$$e_t(\alpha) = 1.000 - 0.780\alpha + 0.840\alpha^2 - 0.210\alpha^3 + 0.028\alpha^4 - 0.022\alpha^5 \quad (5)$$

where the impact angle α is expressed in radians.

The particle density is equal to 2,560 kg/m^3 and the variation of the particle diameter, d_p , is in the range of 0.15 μm – 2.00 μm . All particles are spherical and non-deformable. All the analyses refer to injections having particles with the same diameter, the same material and are thus characterized by the same Stokes number, St (calculated at the inlet of the numerical models). The Stokes number is defined as the ratio of the characteristic time of a particle to a characteristic time of the flow or of an obstacle and explain the physical meaning and the interpretation of its values in the different compressor configurations.

The mass flow rate of the discrete phase, m_p , is linked to the work environment of the compressor (in the case study presented in this paper, typical city side with 100,000,000 particles/ dm^3 as reported by camfil FARR, 2013) and the filtration system efficiency, η_f , (according to Wilcox et al., 2011). For this reason, different values of the total flow rate of contaminants were imposed at the inlet of the compressor.

In order to achieve the uniform particle concentration assumption, particles were released at the same velocity as the freestream (≈ 170 m/s in the case of transonic rotor and ≈ 140 m/s in the case of subsonic rotor). The injection surface (inlet surface) is positioned at about 1.5 chords far from the

rotor in both numerical domains. It is assumed that the particles will not affect the fluid flow (one-way coupling) as the volume fraction of the particles was very low ($\ll 10\%$). All injections took place on a previously-solved flow field, with the compressor operating at the best efficiency point. All results presented in this paper were obtained from converged simulations, with a variation of the residues of the motion (momentum) and turbulent equations close to zero and all lower than 10^{-4} . The injection data are summarized in Table 1 as a function of the rotor.

RESULTS

Capture efficiency.

In this paragraph the analyses of the particle impact on the two rotors are shown. Only a portion of particles injected from the inlet surface of the numerical model impacts on the blade surface, and due to the imposed surface condition (ideal adherence), the contact results in a permanent adherence. For the comparison between the different particle diameters the ratio η_{hit} can be used. The ratio η_{hit} is defined as the ratio between the number of particles that hit the blade and the total number of injected particles. The trends of the η_{hit} as a function of the particle diameter d_p for the two rotors are shown in Fig. 2. It is possible to notice that the percentage of the particles that hit the blade surface increases with the diameter of the particles (solid line) for the two considered rotors. The same result, not shown for brevity, is obtained by comparing these two trends with the trends of the non-dimensional particle relaxation time τ^+ , defined in Eq. 1. The increase of impacting particles with increasing non-dimensional relaxation time is consistent with the indications given in Tian and Hamadi (2006). In Fig. 2, the total number of particles injected and the absolute number of impacting particles on the blade surface are also reported for all studied cases.

From this first analysis it is clearly evident that the transonic rotor could be more affected by the fouling phenomenon because it is more impacted by the particles. As can be seen in Fig. 1, the mass flow rates swallowed by the two rotors are in the same order of magnitude as well as the amount of the contaminant (see Table 1). The higher number of impact showed by the transonic rotor could be due to (i) higher peripheral velocity that leads to higher values of a shear stress on the blade surfaces and to (ii) different fluid dynamic phenomena (such as a separation, shock wave) that leads to different flow fields. Tarabrin et al. (1998b) underline that the sensitivity of the compressor stage to fouling depends mainly on the: (i) chord to tip diameter ratio, (ii) axial component of absolute velocity, (iii) circumferential velocity, (iv) theoretical head, (v) tip diameter and (vi) degree of reaction. Figure 2 shows how the differences in axial compressor performance implies differences in the fouling rate. In the transonic rotor, the shock wave induces higher particle impact. This is due to a thicker boundary layer generated by the flow separation that occurs after the shock wave. Particles reach this blade area because they sweep downstream from the leading edge area due to higher values of shear stress (Kurz and Brun, 2012). Jacobs et al. (2012) have created computer simulations of the dispersion of particles as a result of moving shocks, pointing toward the shock-particle interaction as means of creating particle velocity components perpendicular to the main

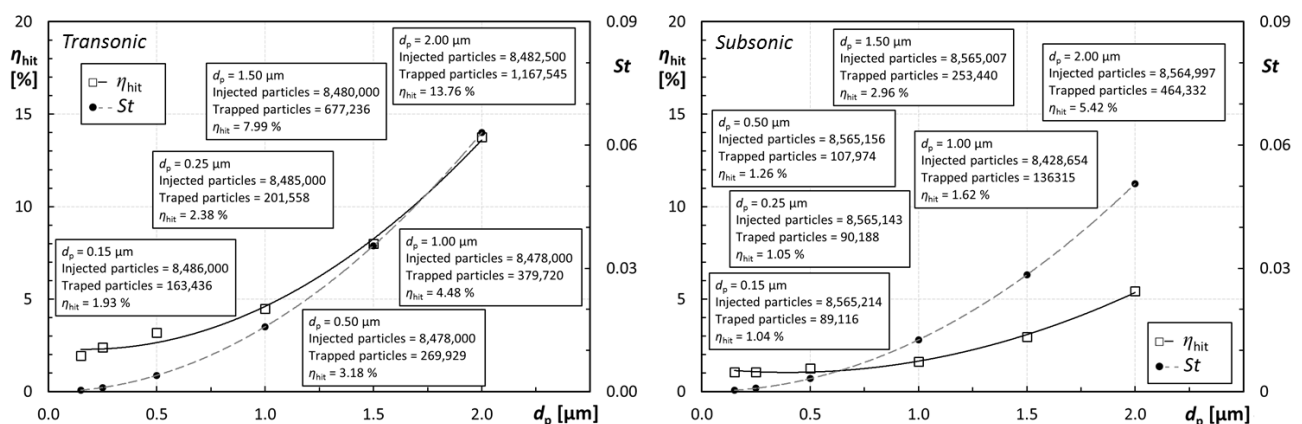


Figure 2 - Capture efficiency η_{hit} and Stokes number St vs particle diameter d_p

flow. So, particle transport perpendicular to the stream lines is greatly promoted by the shock wave. Due to the wall-particle interaction settings, the particles do not stick to the hub and shroud. Particles bounce on these surfaces following the rules imposed by the restitution coefficients reported in Eqs (4) and (5). In Tables 2 and 3, the global count of the bounces is reported. The values of N_b represent the number of particles that bounce on the hub or shroud, the values of n_b represent the ratio between the number of particles that bounce on the hub or shroud and the total number of injected particles and finally, the values of B represent the average number of bounces of each particle. From Table 2, related to the transonic rotor, it can be noticed that the number of bouncy particles increases with the increase of particle diameter but, conversely, the number of average bounces decreases with the increase of particle diameter. This implies that for the smaller diameters, the particles that hit the blade may have had more frequent multiple impacts on the hub or shroud before the impact with the blade. Thus, the smaller particles could have a better chance of sticking to the hub or shroud surface compared to the bigger ones. However, this phenomenon is related to a much smaller number of particles compared to the number of injected particles (less than 2.00 %) and does not influence the overall results. Table 3 reports the values of the bouncing particles in the case of subsonic rotor. Also in this case, the smaller particles have an higher values of average bounces. This phenomenon is related to a much smaller number of particles compared to the number of injected particles (less than 1.00 %) and does not influence the overall results.

Particle impact locations.

In this paragraph, the analysis of the results refers to the impact location of the particles on the blade surface. Noticeable differences can be highlighted regarding the particle impact of the Pressure Side (PS) and Suction Side (SS). Figure 3 reports the trends of the impacting particles on the blade (for both sides and rotors) for all the particle diameters: (i) the η_{hit} values reported for the PS, $\eta_{hit,PS}$, and SS, $\eta_{hit,SS}$, refer to the percentage of particles that hit the PS or SS compared to the total number of injected particles while (ii) the η_{side} values, reported in pie charts, represent the percentage of particles that hit the blade on PS or SS compared to the total number of particles that hit the entire blade. In the case of the transonic rotor, by increasing particle diameter, the SS is less affected by the impacts. There is a greater number of impacts on the PS. As can be seen from Fig. 3, the particles tend to hit the PS in increasing quantities as the particle diameter increases. In the case of the subsonic rotor, by increasing the particle diameter, the number of particles that hit the PS

Table 2 – Particles bounces on the hub and shroud (transonic rotor)

d_p [μm]	Hub			Shroud		
	N_b	n_b [%]	B	N_b	n_b [%]	B
0.15	40,551	0.48	4.1	44,406	0.52	4.5
0.25	66,186	0.78	4.4	66,216	0.78	6.8
0.50	71,154	0.84	2.5	76,236	0.90	6.7
1.00	53,082	0.63	1.3	94,218	1.11	6.4
1.50	63,357	0.75	1.1	122,811	1.45	5.4
2.00	66,186	0.78	4.4	66,216	0.78	6.8

Table 3 – Particles bounces on the hub and shroud (subsonic rotor)

d_p [μm]	Hub			Shroud		
	N_b	n_b [%]	B	N_b	n_b [%]	B
0.15	40,551	0.47	4.1	47,064	0.52	4.5
0.25	41,133	0.48	4.1	47,064	0.55	4.6
0.50	46,053	0.54	3.7	56,208	0.66	4.5
1.00	41,730	0.50	2.1	5,6478	0.67	3.0
1.50	34,143	0.40	1.2	53,241	0.62	2.2
2.00	28,659	0.33	0.7	53,205	0.62	1.8

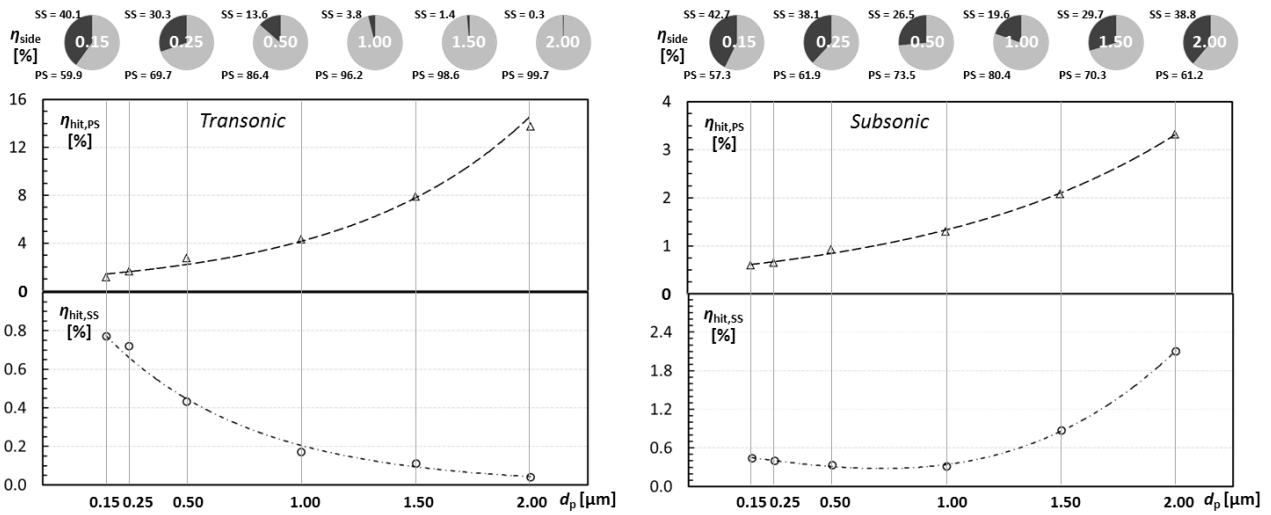


Figure 3 – Particle impact distributions, PS and SS

increases. On the SS, the number of particles that hit the blade decreases up to $d_p = 1.00 \mu\text{m}$, while the number of impacts that take place on the SS increases from $d_p = 1.00 \mu\text{m}$ to $d_p = 2.00 \mu\text{m}$. The transonic rotor is more affected by particle impacts. These impacts take place in greater quantity on the PS, whereas the subsonic rotor shows a more distributed particle impact pattern. These distributions are very important from an operator’s point of view, because the capability of the compressor to collect air contaminants is directly related to the power unit performance drop. In the following paragraphs detailed analyses are conducted in order to show the particle impact locations.

Airfoil impact pattern.

A graphic representation of the particle impact pattern is reported in Fig. 4. Each pattern represents the projection of the fouled airfoil into a perpendicular plane with respect to the spanwise direction. On the upper corner in the left side the spanwise station and the correspondent percentage of the blade span can be seen. The blades were divided into 11 strips along the spanwise direction and each dot on the graph represents a single particle that has hit the blade surface. The upper surface is the SS, while the lower surface is the PS, for each picture.

For both rotors, in the cases with smaller particles (up to $0.50 \mu\text{m}$), the particle impact comprises the entire height of the blade’s SS. In all cases, particles impact at least the first 25 % of the span on

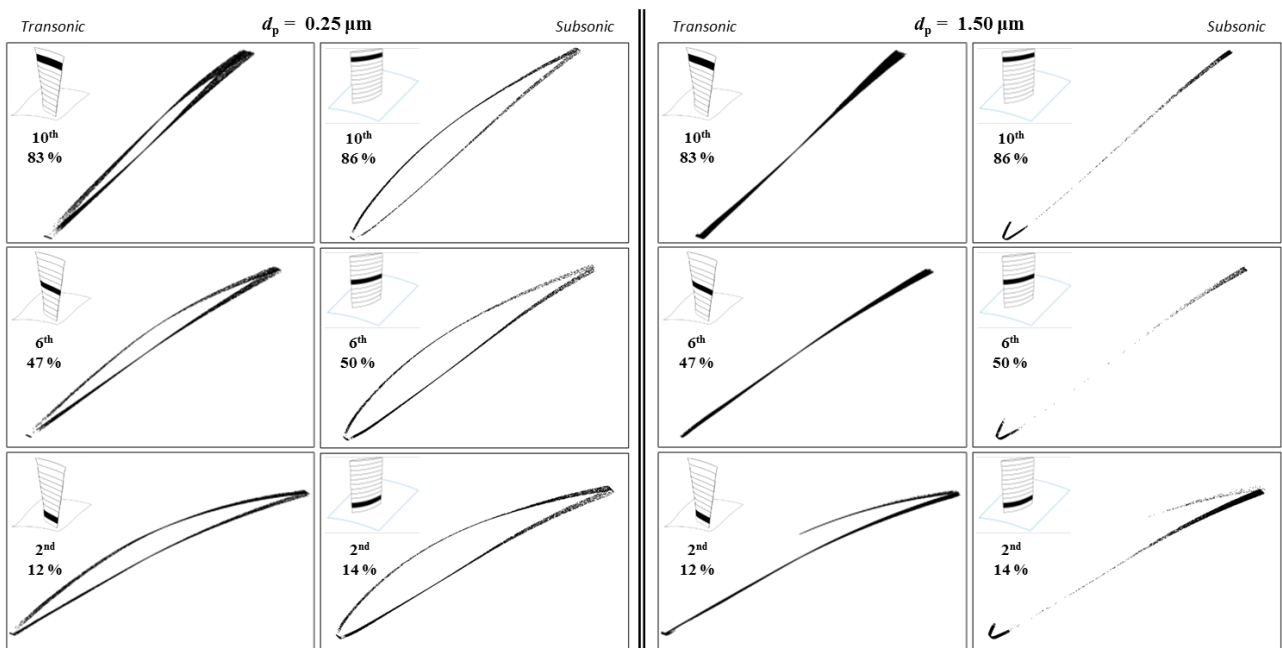


Figure 4 – Airfoil impact patterns, $d_p = 0.25 \mu\text{m}$ and $d_p = 1.50 \mu\text{m}$

the SS. This phenomenon, noticeable in particular for the bigger particles, is due to the flow separation and consequent three-dimensional vortex that drags the contaminants into the vicinity of the hub. Flow separation in the corner region of the blade passage is common (Gbadebo et al., 2005) and strongly influences the particle impact pattern. The differences in the particle impact pattern are more evident for the cases with bigger particles ($d_p > 0.5 \mu\text{m}$), while for the smaller particles the airfoil impact pattern of the two rotors is similar.

Analogous results can be found in Silingardi et al. (2013) where field data regarding the deposition of foulants on a transonic blade compressor are reported. The authors reported the blade surface condition after 25,000 operation hours and the authors highlighted that three-dimensional flow features cause small particles to be deposited in zones where secondary flows and vortices are dominant. The major differences in the particle impact pattern between the rotors are localized in the Leading Edge (LE) zone. For the two rotors, the effect of the stagnation determines the high presence of impacting particles on the LE and, by contrast, there are no particles in the area immediately downstream. The phenomenon is more evident in the transonic rotor, where the velocity field could be characterized by local normal shock waves due to the local curvature of the airfoil (Cumpsty, 1989). The differences in the shape and size of the leading edge, determine differences in the particle impact pattern. The particles can surround the subsonic LE because it is thicker than the transonic LE. In this manner, the subsonic SS appears more contaminated than the transonic SS in particular in the case of bigger particles. These results can clarify the differences highlighted for the trends reported in Fig. 3. The deposition on the leading edge represents a key aspect, because the changes in the LE area (shape, size and surface roughness) represent one of the most important causes of the performance degradation due to fouling (Suder et al., 1995) and erosion (Balan and Tabakoff, 1984).

These results are in line with those reported in literature regarding (i) fouling characterized by particles with dimensions close to the unit of micron (Kurz and Brun, 2012) and (ii) erosion of rotor blades which is characterized by larger particles (Ghenaiet, 2012). In fact, the fouling phenomenon is characterized by a wider distribution of the particles on the blade surfaces with respect to erosion that shows a higher percentage of impacts on the PS than on the SS. As reported in Ahluwalia et al. (1989) inertial deposition takes a place on the pressure surface for diameter greater than $1 \mu\text{m}$ and, by contrast, the suction side is affected by diffusion deposition provided by the diameters less than $1 \mu\text{m}$. In the transonic rotor, where the flow field is greatly different from pressure side and suction side. In the SS the separation due to the shock wave, determine a turbulent and thicker boundary layer. This condition allow the diffusion-deposition condition and, as reported in literature, this condition influence the deposition of the smaller particles (Parker and Lee, 1972). On pressure side, the inertia deposition take a place, and for this reason the impacts increases with the particle diameter. In the subsonic rotor, the flow field on the pressure side and on the suction side is more comparable to each other than in the case of transonic rotor. This situations resulting in very similar impact pattern from PS and SS. The separation and then, diffusion phenomena, take a place only in a small portion of the suction side close to the hub and both blade side show that the inertial deposition is the major contribution in the deposits composition. In particular, as showed above, the deposition is concentrated on the leading edge area and the particle surround the LE from suction side to pressure side.

Particle trajectories.

Figure 5 reports the particle trajectories at the root and at the top of the blade for the two rotors. At the end walls (hub and shroud) the particle trajectories and, in the same way, the fluid dynamic phenomena are quite similar for the two rotors. At the hub, the separation generates a three-dimensional vortex that drags the contaminants into the vicinity of the hub, as mentioned above. At the blade tip the tip leakage vortex drags the particles from the PS to the SS of the blade, as can be seen in Fig. 5. The deposits at the blade tip, especially on the SS, determine the greater performance drop of the compressor. As reported by Aldi et al. (2014), the increased surface roughness and thickness of the airfoil at the blade tip determines a significant work redistribution and greater

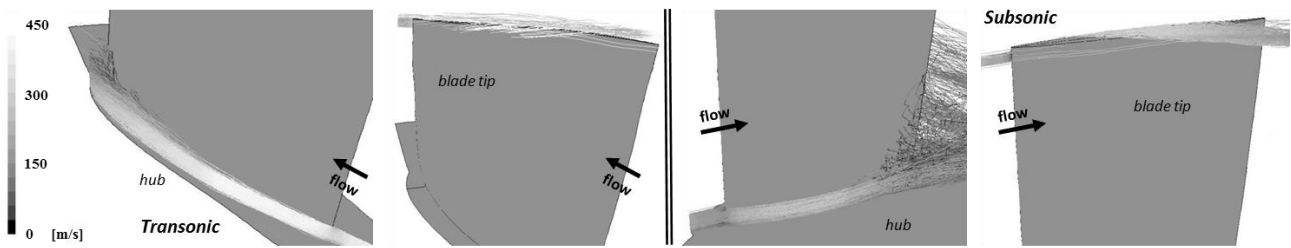


Figure 5 – Particle trajectories at the hub and at the blade tip, $d_p = 0.25 \mu\text{m}$

performance losses.

As reported by Fottner (1989) clearance vortex due to the tip gap (close to the shroud) and corner vortex (close to the hub) determine three-dimensional flow structure of the flow field inside an axial compressor. In a three-dimensional flow field, secondary flows, driven by the flow through tip clearances and the imbalance between the pressure field and the kinetic energy of the air in the boundary layer, have to be considered in the particle impact/deposition analysis. This means in particular, that particles can be deposited in places that would not be reachable for particles in two-dimensional flow.

After these analyses, some general guidelines for proper management of the power unit can be drawn. As reported by Morini et al. (2011) the deposits on the SS have the highest influence on the axial compressor performance drop and for this reason, the filtration system must be designed to remove the smaller particles (up to $0.5 \mu\text{m}$) from the airflow stream because the bigger particles are not able to reach the SS due to their inertia. Compressor fouling is more common and has the more serious effect on engine performance. Typically about 70 % to 85 % of all gas turbine engine performance loss accumulated during operation is attributable to compressor fouling (Diakunchak, 1992, Tarabrin et al., 1998b) and for this reason, a proper filtration system could slow down the gas turbine performance degradation (Diakunchak, 1992, Schroth and Cagna, 2008, Wilcox et al., 2011).

In contrast, on the PS, the particles that could stick do not determine a great performance drop and these deposits could be removed by proper periodic washing operations (Stalder, 2001). Due to this evidence, the water droplets must clean only the PS. The deposits on the LE are easily removed through the washing operation. As reported by Day et al. (2008) all diameter droplets (diameters in the range $50 \mu\text{m} - 200 \mu\text{m}$) surround the LE easily.

CONCLUSIONS

In this paper, an extended comparison on micro-particle ingestion between a transonic rotor and subsonic rotor was carried out. The micro-particles (up to $2 \mu\text{m}$) that are not captured by the air filtration systems determine deposits on the blade surfaces. For this reason, by using a Eulerian-Lagrangian numerical CFD approach, the authors have studied the interaction between fine powder and the blade surface. The numerical model and the particle model have been validated by the experimental and numerical data reported in literature. Special attention was given to the particle-wall interaction in terms of turbulence model wall treatment and in terms of the restitution coefficients. Realistic field data was used for air contaminant concentration, and filtration efficiency.

The key results can be summarized as follows: (i) the percentage of particles that hit the blade surface increases with the diameter of the particles for both rotors and (ii) with the increasing particle diameter the suction side is less affected by the impacts that take place in a greater quantity on the pressure side. The differences in particle impact patterns between the transonic and subsonic rotor are due to (i) the shape of the airfoil and (ii) different fluid dynamic phenomena. In general, the transonic rotor can capture a greater amount of contaminant that concentrates in particular in the pressure side. By contrast, the subsonic rotor is more affected by the contaminant in the areas close to the leading edge and for this reason, the difference between the rotors is more noticeable for the suction side where the bigger particles become more detrimental for the subsonic rotor.

Regarding the management of gas turbine installations, the results of this study highlight the advantage of installing air filtration systems that can remove small and very small particles from the air stream. This would allow the use of effective online washing using larger droplets that typically would only hit and clean the pressure side of the blade.

The understanding of fouling mechanisms in compressors is still a challenge for manufacturers and users. An increase in the knowledge of fouling through the use of numerical codes may therefore constitute a decisive element for better planning of maintenance of turbomachinery.

REFERENCES

- Wilcox, M., Kurz, R., Brun, K., (2011), *Successful Selection and Operation of Gas Turbine Inlet Filtration Systems*” Proceedings of the 40th Turbomachinery Symposium, September 12-15, 2011, Houston, TX, pp. 254-268
- Kurz, R., Brun, K., (2012), *Fouling Mechanism in Axial Compressors*, J. Eng. Gas Turbines Power, **134**, p. 032401
- Tarabrin, A. P., Schurovsky, V. A., Boldrov, A. I., Stalder, J. -P, (1998a), *An Analysis of Axial Compressor Fouling and a Blade Cleaning Method*, J. Turbomach., **120**, pp. 256-261
- Syverud, E., Brekke, O., Bakken, L. E., (2005), *Axial Compressor deterioration caused by Saltwater Ingestion*, J. Turbomach., **129**(1), pp. 119–126
- Suzuki, M., Inaba, K., Yamamoto, M., (2008), *Numerical Simulation of Sand Erosion Phenomena in Rotor/Stator Interaction of Compressor*, J. Therm Sci., **17**(2), pp. 125–133
- Ghenaiet, A., (2012), *Study of Sand Particle Trajectories and Erosion Into the First Compression Stage of a Turbofan*, J. Turbomach., **134**, p. 051025
- Vigueras Zuniga, M. O., (2007), *Analysis of Gas Turbine Compressor Fouling and Washing on Line*, Ph. D. Thesis, Cranfield University, UK
- Parker, G. J., Lee, P., (1972), *Studies of the Deposition of Sub-Micron Particles on Turbine Blades*, Proceedings of the Institution of Mechanical Engineers, **186**(1), pp. 519-526
- Morini, M., Pinelli, M., Spina, P. R., Venturini, M., (2010), *Computational Fluid Dynamics Simulation of Fouling on Axial Compressor Stages*, J. Eng. Gas Turbines Power, **132**(7), p. 072401
- Morini, M., Pinelli, M., Spina, P. R., Venturini, M., (2011), *Numerical Analysis of the Effects of Non-Uniform Surface Roughness on Compressor Stage Performance*, J. Eng. Gas Turbines Power, **133**(7), p. 072402
- Aldi, N., Morini, M., Pinelli, M., Spina, P. R., Suman, A., Venturini, M., (2014), *Performance Evaluation of Non-Uniformly Fouled Axial Compressor Stages by Means of Computational Fluid Dynamics Analyses*, J. Turbomach., **136**, p. 021016
- Suman, A., Kurz, R., Aldi, N., Morini, M., Brun, K., Pinelli, M., Spina, P. R., (2015), *Quantitative CFD Analyses of Particle Deposition on a Transonic Axial Compressor Blade, Part I: Particle Zones Impact*, J. Turbomach., **137**(2), p. 021009
- Reid, L., Moore, R.D., (1978), *Design and overall performance of four highly-loaded, high-speed inlet stages for an advanced high-pressure-ratio core compressor*, NASA TP 1337
- Gosman, A. D., Ioannides, E., (1983), *Aspects of computer simulation of liquid-fuelled combustors*, J. Energy, **7**(6), pp. 482-490
- Tian, T., Ahmadi G., (2006), *Particle deposition in turbulent duct flows — comparisons of different model predictions*, J. Aerosol Sci., **38**, pp. 377-397
- Ahlert, K., (1994), *Effects of Particle Impingement Angle and Surface Wetting on Solid Particle Erosion of AISI 1018 Steel*, M.S. Thesis, Dep. of Mech. Eng., The University of Tulsa, Tulsa, OK
- Fuchs, N. A., (1964), *The Mechanics of Aerosols*, Dover Publications, Inc., New York, US

- Forder, A., Thew, M., Harrison, D., (1998), *A Numerical Investigation of Solid Particle Erosion Experienced Within Oilfield Control Valves*, *Wear*, **216**, pp. 184-193
- camfil FARR, 2013, Technical report
- Tarabrin, W. P., Schurovsky, V. A., Bodrov, A. I., Stalder, J.-P., (1998b), *Influence of Axial Compressor Fouling on Gas Turbine Unit Performance Based on Different Schemes and With Different Initial Parameters*, ASME Paper 98-GT-416.
- Jacobs, G. B., Don, W. S., Dittmann, T., (2012), *High-order resolution Eulerian–Lagrangian simulations of particle dispersion in the accelerated flow behind a moving shock*, *Theor. Comput. Fluid Dyn.*, **26**, pp. 37-50
- Gbadebo, S. A., Cumpsty, N. A., Hynes, T. P., (2005), *Three-Dimensional Separations in Axial Compressors*, *J. Turbomach.*, **127**, pp. 331-339
- Silingardi, A., Astrua, P., Piola, S., Ventrucci, I., 2013, *A Method for a Reliable Prediction of Heavy Duty Gas Turbines Performance Degradation due to Compressor Aging Employing Field Test Data*, Power Gen Europe, June 4-6, 2013, Messe, Wien, Austria
- Cumpsty, N. A., (1989), *Compressor Aerodynamics*, Longman Scientific & Technical, Harlow, UK
- Suder, K. L., Chima, R. V., Strazisar, A. J., Roberts, W. B., (1995), *The Effect of Adding Roughness and Thickness to a Transonic Axial Compressor Rotor*, *J. Turbomach.*, **117**(4), pp. 491–505
- Balan, C., Tabakoff, W., (1984), *Axial flow compressor performance deterioration*, 20th Joint Propulsion Conference, AIAA Meeting paper
- Ahluwalia, R. K., Im, K. M., Wenglarz, R. A., (1989), *Flyash Adhesion in Simulated Coal-Fired Gas Turbine Environment*, *J. Eng. Gas Turbines Power*, **111**, pp. 672-678
- Fottner, L., (1989), *Review of Turbomachinery Blading Design Problems*, Report No. AGARD-LS-167
- Diakunchak, I. S., (1992), *Performance Deterioration in Industrial Gas Turbines*, *J. Eng. Gas Turbines Power*, **114**, pp. 161-168
- Schroth, T., Cagna, M., (2008), *Economical Benefits of Highly Efficient Three-Stage Intake Air Filtration for Gas Turbines*, Proceedings of ASME Paper GT2007-50280
- Stalder, J.- P., (2001), *Gas Turbine Compressor Washing State of the Art: Field Experiences*, *J. Eng. Gas Turbines Power*, **123**, pp. 363-370
- Day, I., Williams, J., Freeman, C., (2008), *Rain Ingestion in Axial Flow Compressors at Part Speed*, *J. Turbomach.*, **130**, p. 011024